

www.acsami.org Research Article

# Piezoelectric Nanocellulose Thin Film with Large-Scale Vertical Crystal Alignment

Jingyu Wang, Corey Carlos, Ziyi Zhang, Jun Li, Yin Long, Fan Yang, Yutao Dong, Xueqing Qiu, Yong Qian,\* and Xudong Wang\*



Cite This: ACS Appl. Mater. Interfaces 2020, 12, 26399–26404



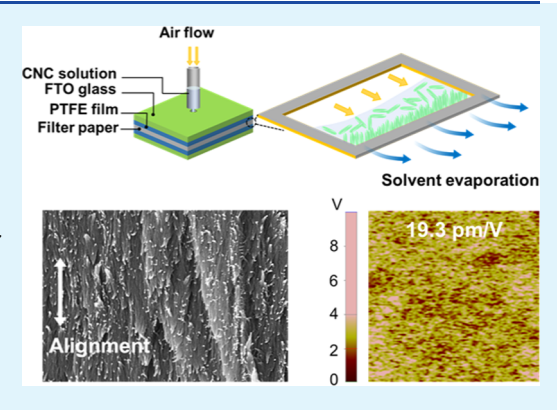
**ACCESS** 

Metrics & More

Article Recommendations

s Supporting Information

**ABSTRACT:** Cellulosic materials are attractive candidates for nature piezoelectrics. Vertically aligned cellulose nanocrystal (CNC) films are expected to show strong piezoelectricity as the largest dipole moment in CNCs exists along the cellulose chain. In this work, we adapted the confinement cell technology that was used to fabricate colloidal opal structures to align CNC rods vertically on a large scale. The high interfacial energy between the CNC-poly(tetrafluoroethylene) (PTFE) surface and torque induced by the shear force led to a large degree to the vertical alignment of CNC rods. An external DC electric field was added to further align the dipole moment of each CNC to the same direction. The as-obtained CNC film displayed excellent piezoelectric performance, and the piezoelectric coefficient was found to be 19.3  $\pm$  2.9 pm/V, comparable to the piezoelectric coefficient  $d_{33}$  of poly(vinylidene difluoride) (PVDF) (20–30 pm/V). This work presents



a new class of high-performance piezoelectric polymeric materials from renewable and biocompatible natural resources.

KEYWORDS: piezoelectricity, cellulose nanocrystal, vertically alignment, polarization, confinement cell

## ■ INTRODUCTION

Since the discovery of piezoelectricity in the 1880s, piezoelectric materials have attracted intensive attention from both academic and industry communities, due to their unique ability to couple mechanical and electrical energy. Nowadays, the rapid evolution of wearable devices is placing a new requirement on piezoelectric materials and devices as biomedical sensors, energy harvesters, and electric stimulators. Novel piezoelectric materials are expected to show desired flexibility, biocompatibility, and degradability. In this emerging area, biomacromolecules, such as cellulose, have been considered as promising candidates for developing advanced piezoelectric materials.

As the most abundant biomass resource on earth, cellulose is featured with nontoxicity, eco-friendliness, biodegradability, and low cost. <sup>6,7</sup> Highly ordered hydrogen-bond networks in crystalline cellulose induce the asymmetric crystalline structure and permanent dipole moments, which is the most important origin of piezoelectricity in cellulose. <sup>8–10</sup> This electromechanical coupling effect of cellulose was first observed in wood. <sup>11</sup> The piezoelectric coefficients of wood are very small (less than 0.3 pm/V) mainly due to the low crystallinity. <sup>12–15</sup> A stronger piezoelectric response was reported in nanocellulose materials, especially in cellulose nanocrystals (CNCs). <sup>16–21</sup> Theoretical calculation of the hydrogen bonds in the unit cell structure suggested that CNCs may possess a piezoelectric coefficient as high as 4–36 pm/V, <sup>10</sup> comparable

to the state-of-the-art commercial piezoelectric polymer materials, e.g., poly(vinylidene difluoride) (PVDF). Nevertheless, the random alignment of CNCs is still the main obstacle for CNC films to show an appreciable piezoelectric performance.

Both experimental and simulated results demonstrated that the largest dipole moment in CNCs existed along the cellulose chain, which was one or two orders of magnitude larger than the dipole moment in the perpendicular direction with respect to cellulose chain. <sup>22,23</sup> Therefore, vertically aligned CNCs with parallel dipole moments would be the ideal configuration to exhibit the strongest piezoelectric performance in bulk form. However, CNC films were only made with a lateral alignment due to the large aspect ratio of the CNCs, which prefers laying down during self-assembly. <sup>24–26</sup> In addition, the dipole moment in the CNC matrix would naturally show antiparallel or random distribution to minimize the internal energy. It is extremely challenging to assemble nanoscale rodlike structures with a vertical alignment and parallel dipole moment. In this paper, we adapted the confinement cell strategy to align CNC

Received: April 3, 2020 Accepted: May 19, 2020 Published: May 19, 2020





rods perpendicular to the film surface by regulating the interfacial energy and shear force and thus stabilized the vertical alignment. To achieve the ideal alignment of CNCs, ethanol was added into CNC aqueous solution to break the chiral nematic structure of CNCs. An external DC electric field was applied to align the CNC dipoles during the assembly process. The vertically aligned CNC film demonstrated a strong piezoelectric response that was comparable to the PVDF film.

### RESULTS AND DISCUSSION

Due to the chiral interaction between CNC particles, stiff and rodlike CNCs could form a stable chiral nematic liquid crystalline structure once the CNC concentration reached a critical volume fraction.<sup>27</sup> The chiral nematic phase is characterized by a long-range order of the rodlike nanostructure with a helical modulation along one direction (Figure 1a).

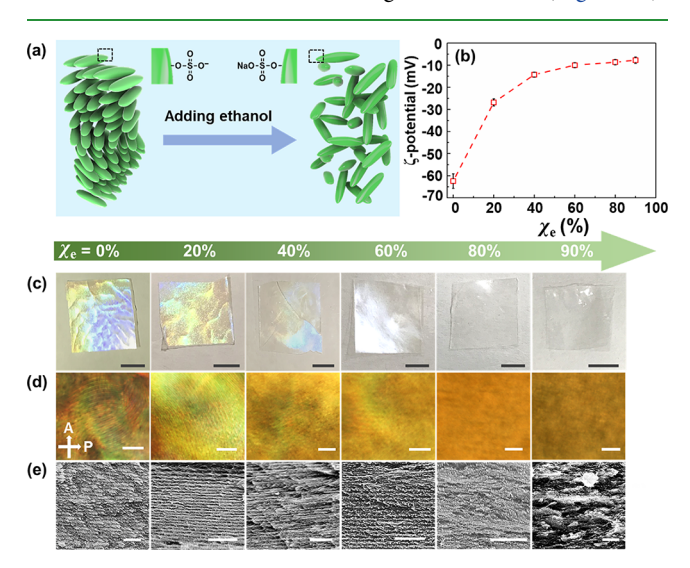


**Figure 1.** Suppressing the formation of a chiral nematic structure in CNC films. (a) Schematic of the chiral nematic structure CNCs. In the presence of ethanol, the ionic sulfate groups  $(-SO_4^-)$  on CNCs are converted to nonionic groups  $(-SO_4Na)$ . Hence, the repulsive force between CNC rods decreased, and thus the chiral nematic structure was suppressed. (b) ζ-Potentials of CNCs in water—ethanol binary solvent at different  $\chi_e$ . The concentration of CNCs was 2 wt % in all cases. (c) Optical photos, (d) POM images, and (e) SEM images (cross-section) of CNC films casted from CNC–water—ethanol dispersions with different  $\chi_e$ . Scale bars are (c) 5 mm, (d) 10 μm, and (e) 1 μm.

This chiral nematic structure could be retained in solid films after drying, which would cancel out the polarization leading to weak or no piezoelectric response in CNC bulk films. To align CNCs along the same direction to achieve desired piezoelectric performance, the nematic chiral structure has to be eliminated.

CNCs extracted from wood cellulose fibers by hydrolysis are always attached with anionic groups such as sulfate or carboxyl groups. Considering the electrostatic repulsion between these anionic groups of CNCs in water being the dominating chiral interaction, ethanol with a mass ratio of  $\chi_e$  was added into CNC aqueous dispersion to minimize the electrostatic interaction, as shown in Figure 1a. Figure 1b shows the  $\zeta$ -potential of CNCs in water—ethanol suspension as a function of  $\chi_e$ . As  $\chi_e$  increases from 0 to 90%, the  $\zeta$ -potential of CNCs changes from -62.4 to -7.7 mV, suggesting that most sulfate

groups were converted from the ionic state (-SO<sub>4</sub><sup>-</sup>) to a nonionic state ( $-SO_4Na$ ). CNC films prepared at different  $\chi_e$ are presented in Figure 1c. CNC films made from solution with small  $\chi_e$  exhibited iridescent color as a result of the chiral nematic structure.<sup>28</sup> As  $\chi_e$  increased to 40%, the iridescent color was significantly reduced, and the film became completely transparent when  $\chi_e$  reached more than 80%. The chiral nematic structure was further confirmed by polarized optical microscopy (POM) and scanning electron microscopy (SEM). As shown in Figure 1d, the POM image revealed clear characteristic helix lines from the films made from CNC-water solution ( $\chi_e = 0\%$ ) and CNC-water-ethanol solution ( $\chi_e = 0\%$ ) 20%). Such helix textures became fuzzier when  $\chi_{\rm e}$  increased to 40%, and completely disappeared when  $\chi_e$  reached 80%. The cross-sections of CNC films were examined by SEM. Obvious helical arrangement was observed from the films with  $\chi_{\rm e}$  of 0 or 20%, where continuous rotation of the CNC plane induced the ordered stripelike textures. As  $\chi_e$  increased from 40 to 80%, the helix structure was gradually changed to disordered arrangement, and then, completely turned into random package when  $\chi_e$  was larger than 80%. All of the characterization methods proved that the chiral nematic structure of CNCs could be completely destroyed by increasing the concentration of ethanol, which was necessary for CNCs to achieve perfect uniaxial vertical alignment.

For vertical alignment of CNC rods, the confinement cell was adapted to introduce a horizontal shear force that generated a torque to rotate CNC rods vertically. The schematic structure of the confinement cell is illustrated in Figure 2a (see details in the experiment section), which consisted of a syringe, two fluorine-doped tin oxide (FTO) glass substrates covered with a poly(tetrafluoroethylene) (PTFE) film, and a filter paper spacer. For the assembly, 2 wt % CNC-water-ethanol ( $\chi_e = 80\%$ ) was used as the chiral structure would not form at this mixture ratio. During the assembly process, CNC solution was slowly injected into the confinement cell through the syringe. Under a constant positive pressure applied by the syringe, the suspension was forced to flow through the edge of the cavity. The filter paper wall with an average pore size of 450 nm (Figure S1) only allowed the solvent to pass through, and CNC rods were packed along the inner wall edge inside the cavity. Three sides of the cavity were sealed by waterproof glue so that the solvent flew along the same direction. The assembly process typically took 2-3 days to complete, and a  $12 \times 5 \text{ mm}^2$  CNC film was obtained along the open edge. To make a clear description in the subsequent discussion, a rectangular coordinate system was set: the direction of liquid flow in the cell was defined as x, and the vertical direction with respect to the substrate was defined

During the assembly, two factors were critical to the vertical alignment of CNC rods: (1) high interfacial energy between the PTFE film and CNCs in water—ethanol solution; and (2) torque of CNC rods induced by shear force. First, the interfacial energy between CNCs and PTFE in water—ethanol ( $\chi_e = 80\%$ ) was found to be 5.1 mJ/m² (Supporting Information, S1). Such a high interfacial energy suggests that CNCs would minimize the contact area with PTFE. Therefore, CNCs easily moved away from both top and bottom surfaces within the cavity, and thus lateral alignment due to flow-induced shear force was not applicable here. Meanwhile, the solvent flew slowly to the spacer edge driven by the evaporation of solvent under air pressure. The liquid flow

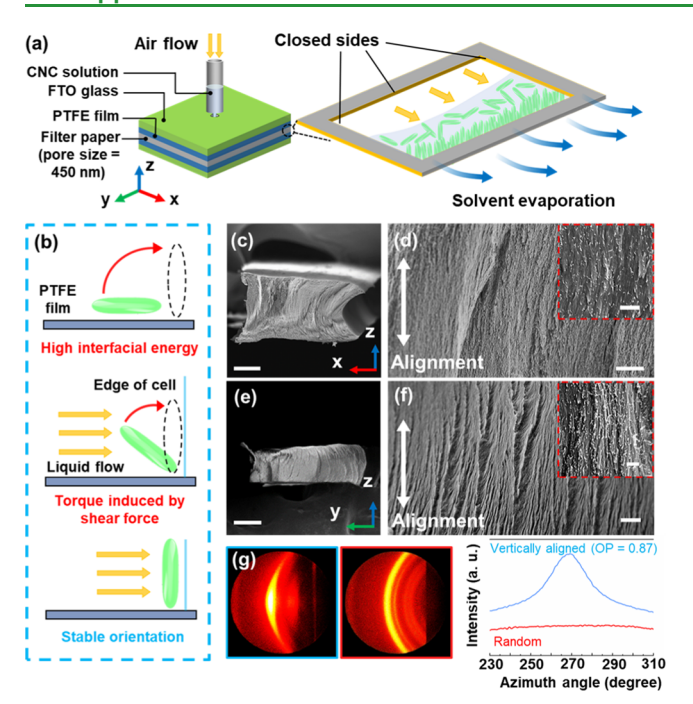


**Figure 2.** Vertical alignment of CNC thin films. (a) Setup of a homemade confinement cell and the alignment process. (b) Schematic of the vertical alignment mechanism. (c–f) Low- and high-magnification SEM images of a vertically aligned CNC film from the z-x plane (c, d) and the z-y plane (e, f). Insets are further zoomed-in SEM images, where vertically aligned individual CNC rods can be observed. Scale bars are (c, e) 50  $\mu$ m, (d, f) 5  $\mu$ m, and inset 200 nm. (g) 2D WAXS patterns of the (200) plane and azimuthal-integrated intensity distribution curves of vertically aligned and isotropic CNC films.

induced a shear force that implemented a torque along the long axis of CNCs. Due to the weak interaction with both substrate surfaces, CNC rods could be easily rotated by the torque and orientated perpendicularly with respect to the movement direction (Figure 2b). Combination of these two effects yielded vertically aligned CNC rods along the open wall edge when the solvent was slowly evaporated.

The morphology images of two different cross-section planes of an as-received CNC film were imaged by SEM. Both x-zand y-z planes showed a densely packed configuration (Figure  $2c_{,e}$ ). The cambered side (-x direction) was induced by the capillary force during solvent drying (Figure 2c). Clearly aligned texture can be observed over all area from the two cross-section images, as shown in Figure 2d,f, respectively. Further zoomed-in images revealed that almost all CNC rods were vertically aligned (inset of Figure 2d,f). The well-aligned structure of the CNC film was further proved by wide-angle Xray scattering (WAXS) measurement, and an isotropic CNC film was prepared by direct casting for comparison. As shown in Figure 2g, the vertically aligned CNC film exhibited a strong (200) plane diffraction pattern (left panel) corresponding to the crystalline phase  $I\beta$  of CNCs. The diffraction showed a concentrated intensity at 22.5°, suggesting that majority of the CNCs were aligned along the same direction, 29,30 whereas the CNC film prepared by direct casting showed a homogeneous (200) diffraction ring pattern corresponding to the random orientation of CNCs in the film (middle panel in Figure 2g). Azimuthal-integrated intensity distribution curves (right panel in Figure 2g) of these two patterns at the (200) plane clearly

revealed the large difference in the preferred vertical orientation between the two CNC films prepared by different approaches. Based on the distribution width of the azimuthalintegrated intensity distribution, the orientation parameter (OP) was calculated to quantify the degree of alignment in CNC films (Supporting Information, S2). The value of OP ranges from 0 to 1, where 0 represents a completely random orientation and 1 represents the perfected uniaxial orientation. The OP of the isotropic film was close to 0, while the OP the vertically aligned CNC film was 0.87. This comparison clearly demonstrated that the confinement cell approach was effective for the fabrication of vertically aligned CNC films. Moreover, the CNC aqueous solution without ethanol ( $\chi_e$  is 0%) was also used to fabricate CNC films by the same method. As shown in Figure S2, although the helix order was slightly changed from the confinement cell assembly, the film still exhibited the chiral nematic structure. This result confirmed that ethanol was necessary to break the chiral nematic structure and obtain vertically aligned CNCs.

While the orientation of CNC rods was largely aligned by the confinement cell technology, in order for the film to show strong piezoelectric responses, it is also essential to have all of the dipole moments in each CNC to be aligned along the same direction. However, as-fabricated vertical CNC films would naturally show random orientation of dipole moments to minimize the internal energy. This random dipole alignment would seriously jeopardize the piezoelectric output of the film. The permanent dipole moment of crystalline cellulose originates from three factors: (1) the polarity of each glucose monomer and the cellulose chain, (2) the intra- and intermolecular hydrogen bonds, and (3) the noncentrosymmetric crystal structure of crystalline cellulose.<sup>22</sup> Among them, hydrogen bonds are most sensitive to external stress or an electric field, and they are the most important factors to the piezoelectric effect in CNCs.9 Figure 3a shows a typical hydrogen bonding network of cellulose I. The intermolecular hydrogen bonds (O6-H···O2) and intramolecular hydrogen bonds (O2-H···O6) contribute a permanent dipole moment along the long axis of CNCs. To align this dipole during the assembly process, a DC voltage of 5 kV was applied to the confinement cell through the two FTO glasses (Figure 3b). The electric field distribution in the confinement cell was simulated by finite element analysis (FEA) (Figure S3). The electric field strength was found to be a uniform 1.3 kV/mm within the cavity when it was filled with CNC-water-ethanol solution ( $\chi_e = 80\%$ ). During the assembly process, the electric field-CNC dipole interaction induced a torque on CNCs, which could rotate the dipole toward the same direction of the electric field. The magnitude of this torque was calculated from eq 1

$$\tau = -pE \sin \theta \tag{1}$$

where  $\tau$  is the magnitude of torque, p is the magnitude of the dipole moment, E is the strength of the electric field, and  $\theta$  is the angle between the dipole and the electric field. It is intuitive that a higher electric field (E) would induce a better alignment of the dipole moment. However, the strength of applied electric field must be controlled below the electrical breakdown limit between the top and bottom electrodes. Therefore, the voltage applied in our assembly system was designed as high as possible without breaking down the device. Figure 3c shows the magnitude of torque on a CNC as a function of dipole moment and  $\theta$ , where  $\theta$  ranged from 0 to

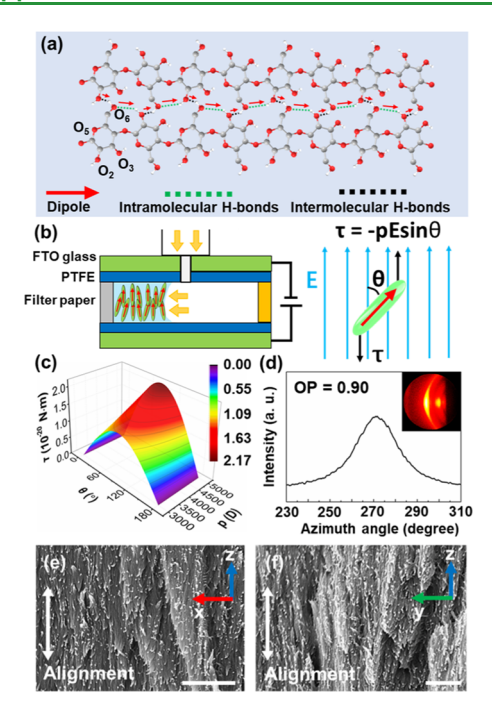


**Figure 3.** Electric dipole alignment in vertical CNC films. (a) Schematic of the hydrogen networks in cellulose  $I\beta$ . The intermolecular hydrogen bonds (O6–H···O2) (black) and intramolecular hydrogen bonds (O2–H···O6) (green) induce a permanent dipole moment in CNCs. (b) Setup of a confinement cell with an external DC electric field. (c) The magnitude of torque on a CNC as a function of dipole moment and  $\theta$ . (d) Azimuthal-integrated intensity distribution curve and 2D WAXS patterns of a vertically aligned CNC film with a parallel dipole moment. SEM images of a vertically aligned CNC film with a parallel dipole moment from the z–x plane (e) and the z–y plane (f). Scale bars are 500 nm.

 $180^{\circ}$  and the dipole moment ranged from 3000 to 5000 debye, which was based on the experimental result measured by rectangular reversing pulse experiments ( $\sim$ 4400 debye). <sup>22</sup> For instance, the torque acted on the CNC with 4000 debye dipole moment is  $1.73 \times 10^{-20}$  N m when its dipole is perpendicular to the electric field ( $\theta$  is 90°). Moreover, the DC electric field could further facilitate the vertical alignment of CNC rods in the confinement cell. The (200) diffraction in the WAXS pattern of an as-received film exhibited a more concentrated intensity (Figure 3d) and the OP value increased from 0.87 to 0.90. SEM images further revealed the good vertical alignment features of CNCs on both cross-sections of x–z and y–z planes, as shown in Figure 3e,f.

The piezoelectric responses were then measured and compared from the vertically aligned CNC films assembled with and without a DC electric field (defined as e-CNC and n-CNC film, respectively) using piezoelectric force microscopy (PFM). Five different areas of the e-CNC films were probed to ensure the representative results (Figure 4a). The PFM phase (Figure 4b) and amplitude images (Figure 4c) were recorded to evaluate the dipole alignment and piezoelectricity strength in the CNC films, respectively, where the degree of phase shift reflects the direction of polarization (Figure 4d). The phase degree image of the n-CNC film showed a wide and symmetric distribution at around 0°, suggesting that the dipole moments of CNCs were random and most of the polarization was canceled out. Accordingly, the PFM amplitude image of the n-CNC film showed a very weak signal map. All of the 5 PFM

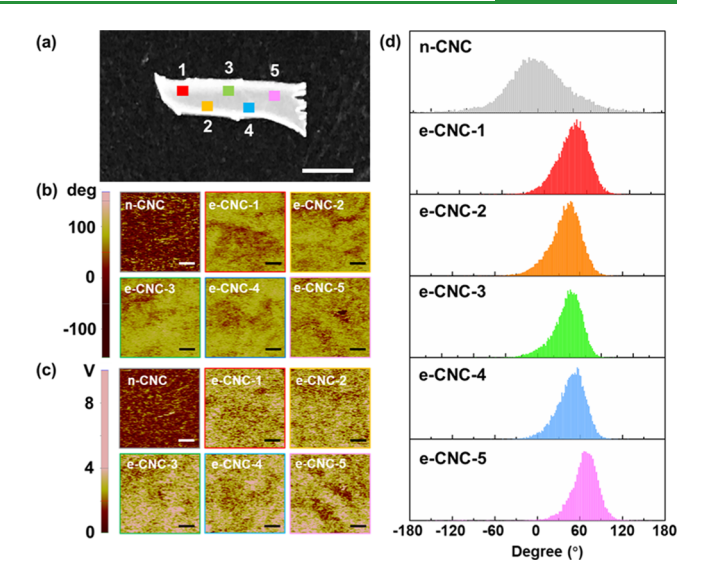


Figure 4. Piezoelectric properties of vertically aligned CNCs. (a) Photo of an e-CNC film. Five different areas are measured. Areas 1–5 are represented by red, orange, green, blue, and pink, respectively. (b) PFM phase images of n-CNC and e-CNC films. (c) PFM amplitude images of n-CNC and e-CNC films. Scale bars are 200 nm. (d) Distribution of the PFM phase shift angle of n-CNC and e-CNC films.

measurements on the e-CNC film displayed a narrow distribution centered at 50–70°, confirming the parallel dipole alignment across the entire assembled CNC film. As a result, strong PFM amplitude maps were obtained from all of the five areas. The piezoelectric coefficients were calculated from the PFM amplitudes for each map and are listed in Table S3 (see the Supporting Information S3 for calculation details). The average piezoelectric coefficient was found to be 19.3  $\pm$  2.9 pm/V, which was close to the  $d_{\rm 33}$  of PVDF films (20–30 pm/V). These results confirmed that the vertical alignment of both CNCs and their dipole orientations is essential to achieve high-performance piezoelectric CNC films.

## CONCLUSIONS

In summary, vertically aligned CNC films with parallel dipole moments were fabricated by a confinement cell technology with the assistance of a DC electric field. To uniaxially align CNCs effectively, an ethanol-water binary solvent was used to suppress the formation of a chiral structure and used for CNC alignment. In the confinement cell assembly process, the high interfacial energy between CNCs and the PTFE surface in ethanol-water solution and the torque induced by the shear force drove the CNC rods rotating to the perpendicular orientation with respect to the substrate and closely packed along the open edge. Both the WAXS pattern and SEM images showed the excellent vertical alignment of CNCs. By adding a 5 kV DC voltage to the confinement cell, the dipole moments were successfully aligned during the vertical assembly process. The as-obtained vertically aligned CNC film exhibited high piezoelectric performance, as obtained from PFM measurements. The average piezoelectric coefficient from the CNC film was calculated to be  $19.3 \pm 2.9 \text{ pm/V}$ , which was close to the piezoelectric coefficient  $(d_{33})$  of a PVDF film. This work presents an effective approach to assemble a CNC film with a high degree for vertical alignment. The as-obtained CNC films will serve as new high-performance piezoelectric polymer films made from renewable and biocompatible natural resources.

### MATERIALS AND METHODS

Preparation of CNC-Water-Ethanol Solution. A CNC suspension with 10.3 wt % in water was obtained from the Forest Products Laboratory in Madison, Wisconsin, United States. Acid hydrolysis was carried out following the procedure included in refs 32, 33. Briefly, the acid hydrolysis was conducted at 45 °C using 62 wt % sulfuric acid. The bleached softwood pulp to acid ratio was 8.75 mg/L, and the reaction time was 45 min. The content of sulfur in dried CNCs is 1.02 wt %. The morphology and XRD pattern of the CNCs was characterized after drying at 60 °C on clean silicon wafer, as shown in Figure S4. The size of the CNC used in this work was around 100–250 nm in length and 5–10 nm in diameter.

To break the nematic chiral structure of CNCs, ethanol was added into CNC aqueous solution.  $\chi_{\rm e}$  represents the mass percentage of ethanol in ethanol—water binary solvent. Certain amounts of distilled water and ethanol were added into the original 10.3 wt % CNC aqueous solution to prepare 2 wt % CNC—water—ethanol solution with the  $\chi_{\rm e}$  values equaling to 0, 20, 40, 60, 80, and 90%, respectively. The CNCs were well dispersed in water—ethanol solution after magnetic stirring for 3 h at 800 rpm.

**Confinement Cell and CNC Alignment.** A homemade confinement cell consisted of a syringe, two FTO glass substrates (3.0 cm  $\times$  3.0 cm  $\times$  2.5 mm) coated with a PTFE film (3.0 cm  $\times$  2.8 cm  $\times$  100  $\mu$ m) and a filter paper spacer (1.5 cm  $\times$  1.5 cm  $\times$  400  $\mu$ m). The conductive sides of both the FTO substrates were facing inside the cavity. The PTFE films were tightly attached to the FTO glass surface as the hydrophobic contact surface. A 4 mm hole was created on the top glass slide. A syringe was fixed to the top slide by fitting the syringe nozzle to the hole and sealed with waterproof glue. A piece of filter paper (obtained from Whatman, WHA7404001) with an average pore size of 450 nm (Figure S1) was cut into a 1.5 cm  $\times$  1.5 cm square frame, and the wall width was 3 mm. This frame was placed in between the two glass slides as a spacer, where three sides were sealed by waterproof glue. The schematic of this device is shown in Figure 2a. A photo of the device is shown in Figure S5.

During the self-assembly process, the confinement cell was held tight by three clips on the three sealed sides. A rubber plug was plugged through the top of the syringe to create a sealed connection with a plastic tube, which was used to provide pressurized air toward the cell cavity. A high voltage DC power supply (30 kV, 10 W) was used to provide an external DC electric field to align the CNC dipoles. The positive and negative outlets were connected to the inside FTO surfaces of bottom and top glasses, respectively, by copper wires. The voltage between the two FTO glasses was slowly increased to 5 kV within 2 min. The inner electric field distribution of the confinement cell was simulated by the commercial finite element analysis (FEA) software ANSYS using the parameters listed in Table S1

In the assembly, 2 mL of 2 wt % CNC-water-ethanol ( $\chi_e = 80\%$ ) was injected into the confinement cell slowly through the syringe. Continuous air pressure was applied through the top of the syringe toward the liquid surface. After 48 h of the assembly process at room temperature, the top substrate was removed carefully. The CNC film was collected from the bottom substrate without any further treatment (Figure S6). The thickness and roughness (Ra) of the CNC film was around 150  $\mu$ m and 16 nm (Figure S7), respectively.

**Characterization.** The piezoelectric response was measured by atomic force microscopy (AFM) (XE-70, Park Systems, South Korea) with the PFM mode. Prior to measurements, the deflection sensitivity of the cantilever was determined. In PFM measurement, a conductive Pt-coated tip (NSC36/Pt-A, Park Systems, South Korea) was approached to contact the surface of the CNC film. The spring constant of this probe is 1.0 N/m, and the radius of curvature of the tip is around 20 nm. A preset AC voltage was applied between the sample surface and the AFM tip to establish an external AC electric field within the film. As a result of the reverse piezoelectric effect, the

CNC film locally expanded or contracted, which generated surface oscillation at the same frequency as the applied AC voltage. The oscillation amplitude was captured by the cantilever deflection, i.e., the PFM amplitude. The shift of the phase degree reflected the polarization orientation. The piezoelectric response could be calculated using the PFM amplitude values (Supporting Information, S3).

AFM topography images were obtained using a noncontact probe (PPP-NCHR, Park Systems, South Korea). The spring constant of this probe was 42 N/m. Scanning electron microscopy (SEM) (LEO 1530, Zeiss, Germany) was utilized to image the morphology of CNC films. Before SEM measurements, all samples were coated with platinum using Leica ACE600 deposition. The  $\zeta$ -potential of CNC—water—ethanol solution was measured by dynamic light scattering (DLS) (Zeta NanoS, Malvern, United Kingdom). Wide-angle X-ray scattering (WAXS) measurement was carried out using D8 discovery (Bruker, Germany). Polarized optical microscopy (POM) images were recorded between crossed polarizers under an optical microscope.

### ASSOCIATED CONTENT

## **Supporting Information**

The Supporting Information is available free of charge at https://pubs.acs.org/doi/10.1021/acsami.0c05680.

Detailed calculation of interfacial energy between the CNC and PTFE; detailed calculation of orientation parameters; detailed calculation of the piezoelectric coefficient; dielectric constants of water, ethanol, water—ethanol binary solvent, and PTFE; surface energy of water, ethanol, water—ethanol binary solvent, CNCs, and PTFE; piezoelectric coefficient of the e-CNC film; AFM, SEM, and XRD of the CNC source; photos of the experimental setup; photos of a vertically aligned CNC film; FEA simulation of the distributions of the electric field and potentials (PDF)

## AUTHOR INFORMATION

### **Corresponding Authors**

Yong Qian — School of Chemistry and Chemical Engineering, South China University of Technology, Guangzhou 510640, P. R. China; orcid.org/0000-0001-9164-5119; Email: ceyqian@scut.edu.cn

Xudong Wang — Department of Materials Science and Engineering, University of Wisconsin-Madison, Madison, Wisconsin 53706, United States; Email: xudong.wang@ wisc.edu

### **Authors**

Jingyu Wang — Department of Materials Science and Engineering, University of Wisconsin-Madison, Madison, Wisconsin 53706, United States; School of Chemistry and Chemical Engineering, South China University of Technology, Guangzhou 510640, P. R. China; orcid.org/0000-0002-8056-2251

Corey Carlos — Department of Materials Science and Engineering, University of Wisconsin-Madison, Madison, Wisconsin 53706, United States

Ziyi Zhang — Department of Materials Science and Engineering, University of Wisconsin-Madison, Madison, Wisconsin 53706, United States; Occid.org/0000-0001-9102-8292

Jun Li – Department of Materials Science and Engineering, University of Wisconsin-Madison, Madison, Wisconsin 53706, United States; Oorcid.org/0000-0002-7498-6736

- Yin Long Department of Materials Science and Engineering, University of Wisconsin-Madison, Madison, Wisconsin 53706, United States; ⊚ orcid.org/0000-0002-6602-0210
- Fan Yang Department of Materials Science and Engineering, University of Wisconsin-Madison, Madison, Wisconsin 53706, United States
- Yutao Dong Department of Materials Science and Engineering, University of Wisconsin-Madison, Madison, Wisconsin 53706, United States
- Xueqing Qiu School of Chemistry and Chemical Engineering, South China University of Technology, Guangzhou 510640, P. R. China

Complete contact information is available at: https://pubs.acs.org/10.1021/acsami.0c05680

#### **Notes**

The authors declare no competing financial interest.

## ACKNOWLEDGMENTS

This work was supported by the University of Wisconsin-Madison, Office of the Vice Chancellor for Research and Graduate Education with funding from the Wisconsin Alumni Research Foundation and National Science Foundation DMR-1709025, and the China Scholarship Council, China (CSC, File No. 201806150081).

## REFERENCES

- (1) Curie, J.; Curie, P. Sur l'électricité polaire dans les cristaux hémièdre à faces inclinées. Présentée par M. Desains. *C. R. Acad. Sci. Gen.* **1880**, *91*, 383–386.
- (2) Rajabi, A. H.; Jaffe, M.; Arinzeh, T. L. Piezoelectric Materials for Tissue Regeneration: A Review. *Acta Biomater.* **2015**, 24, 12–23.
- (3) Wang, X.; Song, W. Z.; You, M. H.; Zhang, J.; Yu, M.; Fan, Z.; Ramakrishna, S.; Long, Y. Z. Bionic Single-Electrode Electronic Skin Unit Based on Piezoelectric Nanogenerator. *ACS Nano* **2018**, *12*, 8588–8596.
- (4) Han, W.; He, H.; Zhang, L.; Dong, C.; Zeng, H.; Dai, Y.; Xing, L.; Zhang, Y.; Xue, X. A Self-Powered Wearable Noninvasive Electronic-Skin for Perspiration Analysis Based on Piezo-Biosensing Unit Matrix of Enzyme/ZnO Nanoarrays. ACS Appl. Mater. Interfaces 2017, 9, 29526–29537.
- (5) Guselnikova, O.; Elashnikov, R.; Postnikov, P.; Svorcik, V.; Lyutakov, O. Smart, Piezo-Responsive Polyvinylidenefluoride/Polymethylmethacrylate Surface with Triggerable Water/Oil Wettability and Adhesion. *ACS Appl. Mater. Interfaces* **2018**, *10*, 37461–37469.
- (6) Miyamoto, T.; Takahashi, S. I.; İto, H.; Inagaki, H.; Noishiki, Y. Tissue Biocompatibility of Cellulose and Its Derivatives. *J. Biomed. Mater. Res.* **1989**, 23, 125–133.
- (7) Moon, R. J.; Martini, A.; Nairn, J.; Simonsen, J.; Youngblood, J. Cellulose Nanomaterials Review: Structure, Properties and Nanocomposites. *Chem. Soc. Rev.* **2011**, *40*, 3941–3994.
- (8) Fukada, E. Piezoelectricity in Polymers and Biological Materials. *Ultrasonics* **1968**, *6*, 229–234.
- (9) Chae, I.; Jeong, C. K.; Ounaies, Z.; Kim, S. H. Review on Electromechanical Coupling Properties of Biomaterials. *ACS Appl. Bio Mater.* **2018**, *1*, 936–953.
- (10) García, Y.; Ruiz-Blanco, Y. B.; Marrero-Ponce, Y.; Sotomayor-Torres, C. M. Orthotropic Piezoelectricity in 2D Nanocellulose. *Sci. Rep.* **2016**, *6*, No. 34616.
- (11) Bazhenov, V. A.; Konstantinova, V. P. Pezoelektricheskie Svoistva Drevesiny. *Dokl. Akad. Nauk SSSR* **1950**, *71*, 283–286.
- (12) Fukada, E. Piezoelectricity of Wood. J. Phys. Soc. Jpn. 1955, 10, 149–154.
- (13) Hirai, N.; Asano, I.; Sobue, N. Piezoelectric Anisotropy of Wood. J. Soc. Mater. Sci., Jpn. 1973, 22, 948–955.

- (14) Hirai, N.; Sobue, N.; Date, M. New Piezoelectric Moduli of Wood: d<sub>31</sub> and d<sub>32</sub>. *J. Wood Sci.* **2011**, *57*, 1–6.
- (15) Fukada, E. Piezoelectricity as A Fundamental Property of Wood. *Wood Sci. Technol.* **1968**, *2*, 299–307.
- (16) Rajala, S.; Siponkoski, T.; Sarlin, E.; Mettänen, M.; Vuoriluoto, M.; Pammo, A.; Juuti, J.; Rojas, O. J.; Franssila, S.; Tuukkanen, S. Cellulose Nanofibril Film as A Piezoelectric Sensor Material. *ACS Appl. Mater. Interfaces* **2016**, *8*, 15607–15614.
- (17) Yang, C.; Kim, J. H.; Kim, J. H.; Kim, J.; Kim, H. S. Piezoelectricity of Wet Drawn Cellulose Electro-Active Paper. *Sens. Actuators, A* **2009**, *154*, 117–122.
- (18) Yun, S.; Jang, S.; Yun, G. Y.; Kim, J. Electrically Aligned Cellulose Film for Electro-Active Paper and Its Piezoelectricity. *Smart Mater. Struct.* **2009**, *18*, No. 117001.
- (19) Yun, S.; Kim, J. H.; Li, Y.; Kim, J. Alignment of Cellulose Chains of Regenerated Cellulose by Corona Poling and Its Piezoelectricity. *J. Appl. Phys.* **2008**, *103*, No. 083301.
- (20) Csoka, L.; Hoeger, I. C.; Rojas, O. J.; Peszlen, I.; Pawlak, J. J.; Peralta, P. N. Piezoelectric Effect of Cellulose Nanocrystals Thin Films. *ACS Macro Lett.* **2012**, *1*, 867–870.
- (21) Hänninen, A.; Sarlin, E.; Lyyra, I.; Salpavaara, T.; Kellomäki, M.; Tuukkanen, S. Nanocellulose and Chitosan Based Films as Low Cost, Green Piezoelectric Materials. *Carbohydr. Polym.* **2018**, 202, 418–424.
- (22) Frka-Petesic, B.; Jean, B.; Heux, L. First Experimental Evidence of a Giant Permanent Electric-Dipole Moment in Cellulose Nanocrystals. *Europhys. Lett.* **2014**, *107*, No. 28006.
- (23) Agarwal, V.; Huber, G. W.; Conner, W. C., Jr.; Auerbach, S. M. Simulating Infrared Spectra and Hydrogen Bonding in Cellulose I $\beta$  at Elevated Temperatures. *J. Chem. Phys.* **2011**, *135*, No. 134506.
- (24) Gan, L.; Feng, N.; Liu, S.; Zheng, S.; Li, Z.; Huang, J. Assembly-Induced Emission of Cellulose Nanocrystals for Hiding Information. *Part. Part. Syst. Charact.* **2019**, *36*, No. 1800412.
- (25) Hoeger, I.; Rojas, Ó. J.; Efimenko, K.; Velev, O. D.; Kelley, S. S. Ultrathin Film Coatings of Aligned Cellulose Nanocrystals from A Convective-Shear Assembly System and Their Surface Mechanical Properties. *Soft Matter* **2011**, *7*, 1957–1967.
- (26) Habibi, Y.; Heim, T.; Douillard, R. AC Electric Field-Assisted Assembly and Alignment of Cellulose Nanocrystals. *J. Polym. Sci., Part B: Polym. Phys.* **2008**, *46*, 1430–1436.
- (27) Lagerwall, J. P.; Schütz, C.; Salajkova, M.; Noh, J.; Park, J. H.; Scalia, G.; Bergström, L. Cellulose Nanocrystal-Based Materials: From Liquid Crystal Self-Assembly and Glass Formation to Multifunctional Thin Films. NPG Asia Mater. 2014, 6, No. e80.
- (28) Revol, J. F.; Godbout, L.; Gray, D. G. Solid Self-Assembled Films of Cellulose With Chiral Nematic Order and Optically Variable Properties. *J. Pulp Pap. Sci.* 1998, 24, 146–149.
- (29) Ye, D.; Lei, X.; Li, T.; Cheng, Q.; Chang, C.; Hu, L.; Zhang, L. Ultrahigh Tough, Super Clear, and Highly Anisotropic Nanofiber-Structured Regenerated Cellulose Films. *ACS Nano* **2019**, *13*, 4843–4853.
- (30) Zhu, M.; Wang, Y.; Zhu, S.; Xu, L.; Jia, C.; Dai, J.; Song, J.; Yao, Y.; Wang, Y.; Li, Y.; Henderson, D.; et al. Anisotropic, Transparent Films With Aligned Cellulose Nanofibers. *Adv. Mater.* **2017**, *29*, No. 1606284.
- (31) Li, J.; Kang, L.; Yu, Y.; Long, Y.; Jeffery, J. J.; Cai, W.; Wang, X. Study of Long-Term Biocompatibility and Bio-Safety of Implantable Nanogenerators. *Nano Energy* **2018**, *51*, 728–735.
- (32) Peng, Y.; Gardner, D. J.; Han, Y.; Kiziltas, A.; Cai, Z.; Tshabalala, M. A. Influence of Drying Method on The Material Properties of Nanocellulose I: Thermostability and Crystallinity. *Cellulose* **2013**, *20*, 2379–2392.
- (33) Beck-Candanedo, S.; Roman, M.; Gray, D. G. Effect of Reaction Conditions on the Properties and Behavior of Wood Cellulose Nanocrystal Suspensions. *Biomacromolecules* **2005**, *6*, 1048–1054.